Multiresolution-Based Rough Fuzzy Possibilistic C-Means Clustering Method for Land Cover Change Detection

Tong Xiao, Yiliang Wan, Jianjun Chen, Wenzhong Shi, Jianxin Qin, and Deping Li

***Abstract*—Object-oriented change detection (OOCD) plays an important role in remote sensing change detection. Generally, most of current OOCD methods adopt the highest predicted probability to determine whether objects have changes. However, it ignores the fact that only parts of an object have changes, which will generate the uncertain classification information. To reduce the classification uncertainty, an improved rough-fuzzy possibilistic *c*-means clustering algorithm combined with multiresolution scales information (MRFPCM) is proposed. First, stacked bitemporal images are segmented using the multiresolution segmentation approach from coarse to fine scale. Second, objects at the coarsest scale are classified into changed, unchanged, and uncertain categories by the proposed MRFPCM. Third, all the changed and unchanged objects in previous scales are combined as training samples to classify the uncertain objects into new changed, unchanged, and uncertain objects. Finally, segmented objects are classified layer by layer based on the MRFPCM until there are no uncertain objects. The MRFPCM method is validated on three datasets with different land change complexity and compared with five widely used change detection methods. The experimental results demonstrate the effectiveness and stability of the proposed approach.**

***Index Terms*—Classification uncertainty, land cover change detection (LCCD), multiresolution segmentation, rough fuzzy possibilistic *c*-means clustering algorithm (RFPCM).**

I. Introduction

LAND cover change detection (LCCD) is the process of finding differences in the state of a geographical object or geographical phenomenon by observing it at different times [1], [2]. LCCD plays an essential role in many fields, such as disaster monitoring [3], environmental protection [4], and earth resource management [5]. It has become one of the most popular applications of remote sensing technology. With the development of satellite technology, there is an increasing number of studies, which use remote sensing images (RSIs) to obtain and monitor land cover change information on the surface of the Earth [6], [7], [8], [9], [10].

Although the increased spatial resolution of RSIs has provided a more convenient and detailed source of data, it has also brought a significant challenge for the traditional pixel-based change detection (PBCD) approach [11]. PBCD approach can obtain "salt and pepper" noise in change detection (CD) maps [12] and results with poor accuracy [13], [14] in RSIs of high-spatial resolution. To overcome the drawback, CD approaches considering spatial information are proposed. Spatial contextual information extraction-based pixel [15], [16] and object-oriented approaches [17], [18] are effective to extract spatial information for RSIs.

The pixel methods based on spatial contextual information use an image block [15], network structure [19], and Markov random field model [20], etc. to obtain spatial information about the pixel context. For instance, Celik[8] proposed the PCA-Kmeans method, which uses "h $\times$ h" image block to explore the spatial contextual information and reduce the noise of CD results. Deep learning-based unsupervised methods, such as MAU-Net [21], GDCN [22], and FDCNN-based CD approach [19] use convolutional network structure to extract the pixel neighborhood information and obtain the change information of the Earth's surface. Lv et al. [23] proposed the hybrid conditional random field to model the spatial information and achieved great CD results. However, it is still a difficult task to detect changes in clarifying the boundaries among different geographic objects [24], which can cause the over-smoothing problem [25].

The object-oriented change detection (OOCD) methods adopt geographic objects as the basic processing unit, which can alleviate the abovementioned problems effectively due to their rich spectrum, shape, spatial, and texture information. Image segmentation plays an essential role in the performance of the OOCD method. Image segmentation aims to obtain "common objects" between bitemporal RSIs in OOCD. Due to the scale effect of RSIs, most of image segmentation algorithms, such as mean shift [26], multiresolution segmentation [27], and fractal

Manuscript received 29 September 2022; revised 24 November 2022; accepted 6 December 2022. Date of publication 12 December 2022; date of current version 21 December 2022. This work was supported in part by the National Natural Science Foundation of China under Grant 42271486, in part by the Humanity and Social Science Youth foundation of Ministry of Education of China under Grant 21YJCZH151 and Grant 20YJC790055, in part by the Natural Science Foundation of Hunan Province, China under Grant 2022JJ30391, in part by the Research Project of Department of Natural and Resources of Hunan Province, China under Grant 2021G08 and Grant 2021–45, and in part by the Changsha City Outstanding Innovative Youth Training Program, China under Grant kq2206025. *(Corresponding author: Yiliang Wan.)*

Tong Xiao, Yiliang Wan, Jianxin Qin, and Deping Li are with the School of Geographical Sciences, Hunan Normal University, Changsha 410081, China, and also with the Hunan Key Laboratory of Geospatial Big Data Mining and Application, Hunan Normal University, Changsha 410081, China (e-mail: xttx2020@smail.hunnu.edu.cn; wanylir@hunnu.edu.cn; 12495@hunnu.edu.cn; lideping106@aliyun.com).

Jianjun Chen is with the Hunan Vocational College of Engineering, Changsha 410151, China (e-mail: 303159496@qq.com).

Wenzhong Shi is with the Department of Land Surveying and Geo-Informatics, The Hong Kong Polytechnic University, Hong Kong 999077, China (e-mail: lswzshi@polyu.edu.hk).

Digital Object Identifier 10.1109/JSTARS.2022.3228261

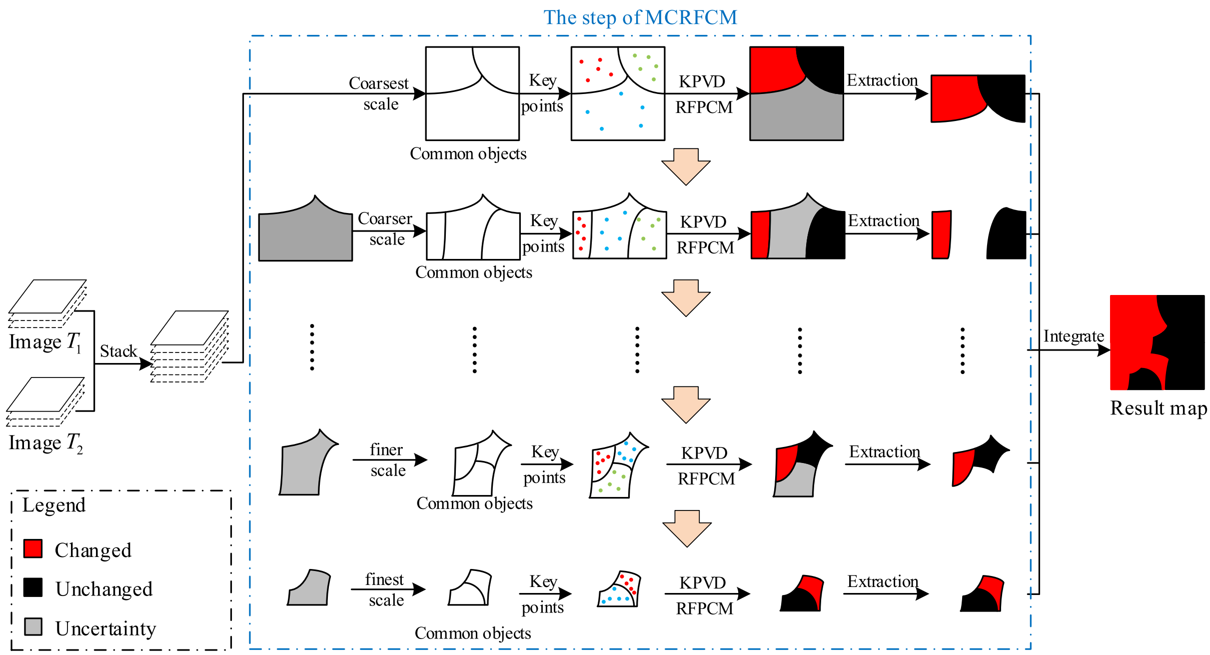

Fig. 1. Flowchart of the LCCD approach based on the proposed MRFPCM.

net evolution approach [28] acquire geographic objects at a specified scale. Many studies focused on how to find the best scale in segmentation by comparing the CD results with different scale parameters [29], [30], [31] or by using the existing segmentation evaluation index [32]. Nevertheless, the single-scale information greatly limits the generalization ability of the CD algorithm, particularly in RSIs with complex changes and significant differences in feature size scales. Therefore, CD methods combining feature information from different scales are developed, which could break the abovementioned limitation and improve CD accuracy [33], [34].

After image segmentation, classifiers are employed to classify objects into changed and unchanged categories. Classification methods usually have two branches in unsupervised methods: threshold and clustering methods. Threshold methods, such as maximum entropy thresholding [35], fuzzy thresholding [36], and OTSU [37] obtain changed and unchanged feature objects by automatically dividing thresholds [38], [39]. Meanwhile, clustering approaches including K-means [40], fuzzy c-means [41], and Gaussian mixture model [42] acquire changed and unchanged clusters by calculating the proximity of distances [43]. However, the category with the highest predicted probability is regarded as the final category in the abovementioned approaches, which can introduce uncertainties when the predicted probabilities of the changed and unchanged are close [44]. For instance, P_c and P_u represent the probability of an object belonging to changed and unchanged, respectively (P_c is greater than P_u). If the difference between P_c and P_u is significant, it is reasonable to determine the geographic object as changed. However, it is likely that only parts of the object have changed while P_c is pretty close to P_u.

To address the aforementioned problems, this article proposes an improved multiresolution-based on rough fuzzy possibilistic c-means clustering approach (MRFPCM) to reduce the classification uncertainty layer by layer. A state-of-the-art change characteristics extraction method, key point vector distance (KPVD) [24], is employed to measure the change magnitude between the pairwise objects. Then, MRFPCM is applied in three pairs of RSIs with different change complexity to test the stability and reliability of the algorithm. In the end, five widely used CD methods, namely, CVA [45], MAD [46], PCA-Kmeans [8], SFA [47], and KPVD-based [24] are compared with the proposed method to evaluate its feasibility.

The rest of this article is organized as follows. Section II provides a comprehensive description of the proposed MRFPCM method. Section III presents the experiments and analysis. Some discussions on the proposed method are presented in Section IV. Finally, Section V concludes this article.

II. Methodology

The proposed method integrates the information from multiple scales and employs the improved rough fuzzy possibilistic c-means clustering (MRFPCM) approach to reduce the classification uncertainty layer by layer. As shown in Fig. 1, the proposed MRFPCM approach comprises the following steps.

1) Select a series of scale parameters from coarse to fine. Stacked bitemporal images are segmented to generate “common objects” at the coarsest scale.
2) KPVD is used to measure the change magnitude between bitemporal objects. Then, the improved RFPCM (MRFPCM) approach classifies bitemporal objects into changed, unchanged, and uncertain objects based on change magnitudes.
3) The uncertainty objects are segmented at a fine scale. The MRFPCM approach recalculates the change magnitude

centers (CMCs) of the changed and unchanged from the objects at the previous scales as the training data and classifies the uncertain objects into changed, unchanged, and uncertain objects. The changed and unchanged objects at the fine scale would be combined with the changed and unchanged objects at all the previous scales to generate new CMCs of changed objects at a finer scale.

4) Step 3) is repeated until all the uncertain objects are classified into changed and unchanged categories.
5) Integrate all the changed and unchanged objects from the different scales to generate the CD results.

A. Multiresolution Segmentation Method

Image segmentation is the process of converting RSIs into discrete regions or objects with uniform spatial or spectral characteristics [27], [29]. Due to the complexity of the geographic objects, it is difficult to describe them at a specific scale and a single image in bitemporal images. To generate the "common objects" at different scales, the multiresolution segmentation method in eCongnition 9.0 is applied in this article. The multiresolution segmentation method has the following advantages: 1) it can generate different objects using the scale parameter, which is essential to control the internal (spectral) heterogeneity of objects; 2) it can use the stacked bitemporal image information as the image layer weights parameters [28], [48], [49]. In order to achieve the spectral and shape features of geographical objects in different periods, two RSIs in different periods are combined into one stacked bitemporal image. Subsequently, the stacked bitemporal image information is segmented into "common objects" from different scales by the multiresolution segmentation method.

B. Key Point Vector Distance (KPVD)

To describe the discrete and biased characteristics of the spectral values within an object in RSIs, the key point vectors (KPVs) of an object is generated by employing a set of interest pixels to characterize the characteristics of an object instead of considering all its pixels [24]. The steps for obtaining the key points are as follows. First, the spectral values of an object in a specific band are sorted from smallest to largest, denoted as set A. Second, five points including the minimum, lower quartile, median, upper quartile, and maximum values in set A are selected, which are represented as k_0, k_1, k_2, k_3, and k_4, respectively.

Based on the selection of KPV, the KPVD can be calculated as follows:

$$\Delta d_i = \frac{1}{2\times m}\sum_{l=1}^{l=m} ||\mathrm{KPV}_i^{t_1}(l) - \mathrm{KPV}_i^{t_2}(l)|| \tag{1}$$

$$\Delta d_i = \frac{1}{2\times m\times 5}\sum_{l=1}^{l=m}\sum_{j=1}^{j=5} ||k_j^{t_1}(l) - k_j^{t_2}(l)|| \tag{2}$$

where Δd_i is the change magnitude of the object i from t_1 to t_2; m is the number of spectral bands in one of the bitemporal images; l indicates a specific band in the image; j represents the jth element within a KPV; $\frac{1}{2}||\mathrm{KPV}_i^{t_1}(l) - \mathrm{KPV}_i^{t_2}(l)||$ indicates KPVD between two objects in the l-band and $\frac{1}{2}||k_j^{t_1}(l) - k_j^{t_2}(l)||$ represents the distance between two objects using the jth KPV element in the l-band.

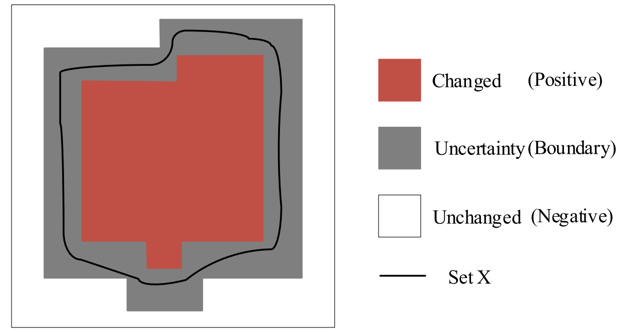

Fig. 2. Concept map of rough set in CD.

C. Rough Fuzzy Possibilistic C-Means Clustering Algorithm (RFPCM)

The RFPCM method introduces rough-set theory based on the possibilistic C-means (PCM) method [50]. The rough sets theory was proposed by Pawlak [51], and it could deal with uncertainty in class definition of CD. Let a pair $< U, R >$ be an approximation space, where $U = \{u_1, \ldots u_j, \ldots u_n\}$ is the set of n objects, and R is an equivalence relation on U. Let U/R represents the quotient set of U by the equivalence relation R, and $U/R = \{X_1, \ldots X_m, \ldots X_v\}$, where X_i is an equivalence class of R, $i = 1, \ldots m, \ldots v$. For an equivalence class X, the lower and upper approximations ($\underline{R}(X)$ and $\overline{R}(X)$) are defined as follows:

$$\underline{R}(X) = \bigcup_{X_i \subseteq X} X_i \tag{3}$$

$$\overline{R}(X) = \bigcup_{X_i \bigcap X \neq \oslash} X_i. \tag{4}$$

Based on the concept of lower and upper approximations, the positive, negative, and boundary regions of X for the equivalence relation R ($\mathrm{POS}_R(X)$, $\mathrm{NEG}_R(X)$, and $\mathrm{BND}_R(X)$) are defined as follows:

$$\mathrm{POS}_R(X) = \underline{R}(X) \tag{5}$$

$$\mathrm{NEG}_R(X) = U - \overline{R}(X) \tag{6}$$

$$\mathrm{BND}_R(X) = \overline{R}(X) - \underline{R}(X). \tag{7}$$

The concept of positive, negative, and boundary regions can solve the uncertainty of the classification in the CD based on RSIs. As shown in Fig. 2, the positive region indicates that there is high confidence that the objects are changed; conversely, the negative region means that objects are likely to be unchanged; and the boundary region represents that it is uncertain to determine whether objects are changed or unchanged. Based on the positive, negative, and boundary regions, the RFPCM algorithm divides U into c clusters by minimizing the objective function

$$J_i = J\begin{cases}\omega \times A_1 + (1-\omega) \times B_1, & \text{if } \text{POS}_R(X) \neq \oslash \\ & \text{BND}_R(X) \neq \oslash \\ A_1, & \text{if } \text{POS}_R(X) \neq \oslash, \text{BND}_R(X) = \oslash \\ B_1, & \text{if } \text{POS}_R(X) = \oslash, \text{BND}_R(X) \neq \oslash. \end{cases} \quad (8)$$

$$A_1 = \sum_{i=1}^{i=c} \sum_{x_j \in \text{POS}_R(X)} a(\mu_{ij})^{m_1} + b(\upsilon_{ij})^{m_2} ||x_j - V_i|| + \sum_{i=1}^{i=c} \eta_i \sum_{x_j \in \text{POS}_R(X)} (1-\upsilon_{ij})^{m_2} \quad (9)$$

$$B_1 = \sum_{i=1}^{i=c} \sum_{x_j \in \text{BND}_R(X)} a(\mu_{ij})^{m_1} + b(\upsilon_{ij})^{m_2} ||x_j - V_i|| + \sum_{i=1}^{i=c} \eta_i \sum_{x_j \in \text{BND}_R(X)} (1-\upsilon_{ij})^{m_2} \quad (10)$$

where ω is the relative importance of lower approximation region; m_1 and m_2 indicate the fuzzifiers (generally, $m_1 = m_2 = 2$); a and b are the constants which represent the relative importance of probabilistic membership μ_{ij} and possibilistic membership υ_{ij}. Therefore, the following equations can be obtained:

$$\begin{aligned} a + b &= 1 \\ \mu_{ij} &= \left(\sum_{k=1}^{k=c} \left(\frac{d_{ij}}{d_{kj}}\right)^{\frac{2}{m_1-1}}\right)^{-1} \\ d_{ij}^2 &= ||x_j - \upsilon_i||^2 \\ \upsilon_{ij} &= \frac{1}{1+E} \\ E &= \left\{\frac{b||x_j - \upsilon_i||^2}{\eta_i}\right\}^{\frac{1}{(m2-1)}} \end{aligned} \quad (11)$$

where η_i represents the zone of influence of cluster X; υ_i indicates the center of the cluster. The calculations are as follows:

$$\eta_i = \frac{\sum_{j=1}^{j=n} (\upsilon_{ij})^{m_2} ||x_j - \upsilon_i||^2}{\sum_{j=1}^{j=n} (\upsilon_{ij})^{m_2}} \quad (12)$$

$$\upsilon_i^{\text{RFP}} = \begin{cases}\omega \times C_1 + \varpi \times D_1, & \text{if } \text{POS}_R(X) \neq \oslash \\ & \text{BND}_R(X) \neq \oslash \\ C_1, & \text{if } \text{POS}_R(X) \neq \oslash, \text{BND}_R(X) = \oslash \\ D_1, & \text{if } \text{POS}_R(X) = \oslash, \text{BND}_R(X) \neq \oslash \end{cases} \quad (13)$$

where C_1 and D_1 indicate changed and unchanged regions, which are defined as follows:

$$C_1 = \frac{1}{|\text{POS}_R(X)|} \sum_{x_j \in \text{POS}_R(X)} x_j$$

$$D_1 = \frac{\sum_{x_j \in \text{BND}_R(X)} \{a(\mu_{ij})^{m_1} + b(\upsilon_{ij})^{m_2}\} \times x_j}{\sum_{x_j \in \text{POS}_R(X)} \{a(\mu_{ij}^{m_1}) + b(\upsilon_{ij}^{m_2})\}}. \quad (14)$$

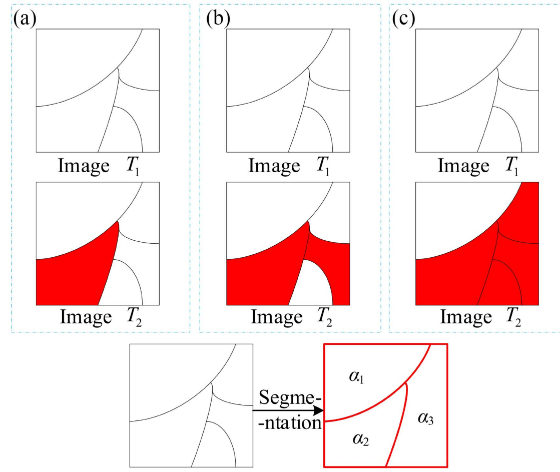

Fig. 3. Three hypothetical cases based on the MRFPCM approach. (The black contour line means the real boundary of the object, the white fill color indicates the real unchanged object, the red fill color represents the real changed object, and the red contour line implies the common objects after segmentation.).

The key to solving (8) is to determine whether x_j belongs to $\underline{R}(X)$ or $\overline{R}(X)$. Classical RFPCM used a fixed threshold threshold to classify the objects into two categories: changed, unchanged, and uncertainty. μ_c and μ_u are the memberships of an object belonging to the changed and unchanged categories. If $(\mu_c - \mu_u)$ is greater than a threshold T, the object belongs to the changed categories; if $(\mu_u - \mu_c)$ is greater than T, the object belongs to the unchanged categories; otherwise, it belongs to the uncertain categories.

D. Multiresolution-Based Rough Fuzzy Possibilistic C-Means Clustering Algorithm (MRFPCM)

The above RFPCM method applies to the PBCD method but does not extend it to the OOCD method. Inspired by the RFPCM method and the uncertainty-refining strategy layer by layer [33], an improved RFPCM approach combined with multiresolution information (MRFPCM) is proposed to reduce the classification uncertainty in the OOCD method.

In image segmentation, there exist some incompletely segmented objects, which can make it difficult to determine whether they are changed or not. As shown in Fig. 3, there are three hypothetical cases with two images in T_1 and T_2: case A), the tiny object on the right side has not changed; case B), only one tiny object on the right has changed; case C), the tiny object on the right side has changed. Two images are segmented at a specific scale to obtain the common object, the results in the tiny object on the right side of the image not being completely segmented. α_1, α_2, and α_3 represent change magnitude of three objects between two periods. According to the real change of the ground surface, we assume $\alpha_1 \approx \alpha_3 < \alpha_2$ in case A), $\alpha_1 < \alpha_3 < \alpha_2$ in case B), and $\alpha_1 < \alpha_2 \approx \alpha_3$ in case C). Most of the classification methods can accurately classify in cases A) and C). However, it is difficult to classify the images in case B) based on the predicted probabilities due to the partial change in the geographical object.

To overcome the drawback, a shrinkable threshold variable and the uncertainty-refining strategy layer by layer are introduced into the RFPCM method. The improved RFPCM approach adopts a shrinkable threshold variable to classify the image into the following three categories: changed, unchanged, and uncertainty. The threshold will gradually decay as segmentation scales decrease. Then, the uncertainty will be reclassified into three categories at a fine scale. To integrate the multiresolution information, the CMCs of the changed and unchanged will be recalculated based on the previous changed and unchanged objects. By this improved method, the objects of the case B) with the change magnitude α_1 and α_2 will be classified into the changed and unchanged categories, while the object with α_3 into the uncertain category. Additionally, in case A), the objects with α_1 and α_3 will be determined as the unchanged category, and the object with α_2 will be classified into the changed category by this method. In case C), the improved MRFPCM approach will classify the object where the value of α_2 and α_3 into the changed category.

1) Shrinkable Membership Threshold: The improved RF-PCM approach uses a membership threshold to indicate that objects have great confidence in being classified as changed categories. At the coarsest scale, an initial threshold is set to classify objects as changed, unchanged, and uncertain categories. Then, the uncertain objects will be segmented into tiny objects, and the tiny objects will be continuously classified as new changed, unchanged, and uncertain categories. In this classification, if the initial threshold is not changed, there will always be uncertain objects no matter how many times doing segmented. Therefore, a threshold decay strategy is set to remove the uncertain categories at a special scale. The formula for threshold classification and decay is as follows:

$$\begin{aligned} \text{POS}_R(i\_n) &= \mu_{ic\_n} > \epsilon_n \\ \text{NEG}_R(i\_n) &= \mu_{ic\_n} < 1-\epsilon_n \\ \text{BND}_R(i\_n) &= \mu_{ic\_n} > 1-\epsilon_n \quad \text{and} \quad \mu_{ic\_n} < \epsilon_n \\ \epsilon_n &= \epsilon - (n-1) \times \eta \end{aligned} \tag{15}$$

where n and i represent the nth segmentation and the ith object, respectively; μ_{ic_n} is the membership of the ith object belonging to the change category in the nth segmentation; ϵ_n denotes the threshold value of the nth segmentation, ϵ denotes the initial threshold; η is the fuzzy reduction factor. While ϵ_n is equal to 0.5, all the objects will be divided into changed and unchanged classes. There are two cases where ϵ_n is equal to 0.5: natural decay to 0.5 and segmentation to the finest scale. For the second case, although ϵ_n is greater than 0.5, there is no finer scale information. Therefore, to classify all objects into changed and unchanged categories, ϵ_n is changed to 0.5.

2) CMCs Based on Multiresolution Information: To describe the CMCs comprehensively, the information at different scales should be integrated. Therefore, we combine the changed and unchanged objects at the current scale and all the previous scales. Subsequently, the CMCs of the changed and unchanged classes at a finer scale are calculated based on the integrated changed and unchanged objects. By (15), new changed and unchanged objects are classified based on the calculated CMCs of the changed and unchanged classes. The calculations are defined as follows:

$$\begin{aligned} v_{n\_c\_\text{mean}} &= \frac{v_{n-1\_c\_\text{mean}} \times m + v_{n\_c} \times n}{m+n} \\ v_{n\_\text{unc\_mean}} &= \frac{v_{n-1\_\text{unc\_mean}} \times p + v_{n\_\text{unc}} \times q}{p+q} \end{aligned} \tag{16}$$

where $v_{n\_c\_\text{mean}}$ and $v_{n\_\text{unc\_mean}}$ are the CMCs of all changed and unchanged objects after nth segmentation, respectively; m is the number of all changed objects after $(n-1)$th segmentation; v_{n_c} and v_{n_unc} are the CMCs of changed and unchanged objects at the nth segmentation scale, respectively; n is the number of changed objects at nth segmentation scale; p represents the number of all unchanged objects after $(n-1)$th segmentation; q represents the number of unchanged objects at nth segmentation scale.

E. Evaluation Indicators

To evaluate the accuracy of the proposed MRFPCM, four popular evaluation indicators, including false alarm (FA), missed alarm (MA), total error (TE), and binary classification Kappa coefficient (Ka) are employed [15]. The calculation equations are as follows:

$$\begin{aligned} \text{FA} &= (\text{FP}/(\text{TP}+\text{FN})) \\ \text{MA} &= (\text{FN}/(\text{TP}+\text{FN})) \\ \text{TE} &= (\text{FP}+\text{FN})/(\text{TP}+\text{TN}+\text{FP}+\text{FN}) \\ \text{Ka} &= \frac{2 \times (\text{TP} \times \text{TN} - \text{FN} \times \text{FP})}{k_1 \times k_2 + k_3 \times k_4} \end{aligned} \tag{17}$$

where the true positive (TP) and false negative (FN) indicate that the detected results are actually changed and unchanged in the real case that the pixel is changed, respectively; the true negative (TN) and false positive (FP) represent that the detected results are actually unchanged and changed in the real case that the pixel is unchanged, respectively; $k_1 = \text{TP} + \text{FP}$, $k_2 = \text{FP} + \text{TN}$, $k_3 = \text{TP} + \text{FN}$, $k_4 = \text{FN} + \text{TN}$. In addition, FA denotes the ratio between the number of incorrectly identified change pixels in the CD map and the ground reference map; MA means the ratio between the number of missing change pixels in the CD map and the ground reference map; TE demonstrates the ratio of the total number of FA and missing detections to the total number of pixels in the ground reference map; Ka measures the internal reliability of the qualitative items of detection results with a threshold value between 0 and 1.

III. Experiments

A. Data Description

As shown in Fig. 4, three pairs of RSIs with different levels of change complexity are used to verify the reliability and stability of the proposed method. Dataset I includes two Landsat 7 images with 400×400 pixels, which were acquired in Liaoning Province in August 2001 and August 2002, respectively. The spatial resolution of the bitemporal images was 30 m/pixel, and the changed lands are farmland, which means that the changes in dataset I are relatively homogeneous and straightforward. The datasets II and III with a high-spatial resolution of 0.5 m/pixel

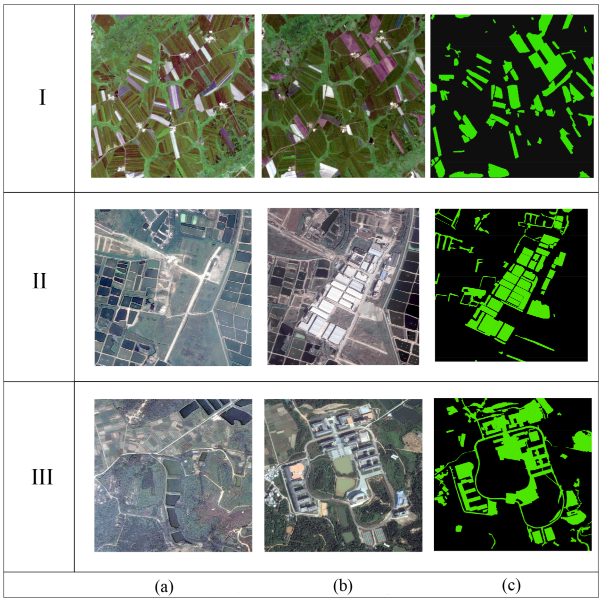

Fig. 4. Datasets and their preference map. From top to bottom, the complexity of geographic objects or phenomenon change becomes higher. (a) Image T_1. (b) Image T_2. (c) Reference map.

are both Google Earth images in Guangzhou, China. The images of dataset II with 1836×1836 pixels were collected in June 2015 and December 2017, respectively, and the types of the changed lands mainly include bare land, forest land, buildings, and roads. Dataset III with 1360×1316 pixels were collected in September 2006 and October 2014, respectively. The changed land types of dataset III are mainly bare land, forest land, buildings, ponds, and roads. Datasets II and III have a higher complexity of feature changes compared to dataset I. These datasets can help to test the stability of the proposed method for different complexities of land changes.

In addition, the ground reference map of each dataset was manually interpreted in ArcGIS 10.6 software.

B. Experimental Setup

Five LCCD approaches, including a traditional pixel-based approach, three kinds of change magnitude description or spatial context enhanced pixel-based approaches, and one widely used object-oriented approaches, namely, CVA [45], MAD [52], PCA-Kmeans [8], SFA [47], and KPVD-based [24] are compared with the proposed MRFPCM approach to evaluate its effectiveness.

In the parameters setting of image segmentation, the bands used for the three datasets are red, green, and blue bands, and the weight of each band layer was 1. In addition, the shape and compactness indices are set to 0.1 and 0.5 for all the datasets, respectively; the scale parameters for the KPVD-based approach are 10, 50, and 30 for datasets I, II, and III, respectively. According to the sensitivity analysis, the coarsest segmentation scales for the three datasets are 10, 50, and 30, and the initial membership thresholds are set to 0.90, 0.70, and 0.85 in the proposed MRFPCM, respectively. The finest scales for datasets I, II, and III are set to 5, 20, and 20 based on the complexity and the spatial resolution of the data. The scale and threshold are reduced by 5 and 0.50 for each segmentation. The other parameters involving shape and compactness were the same as the KPVD-based approach.

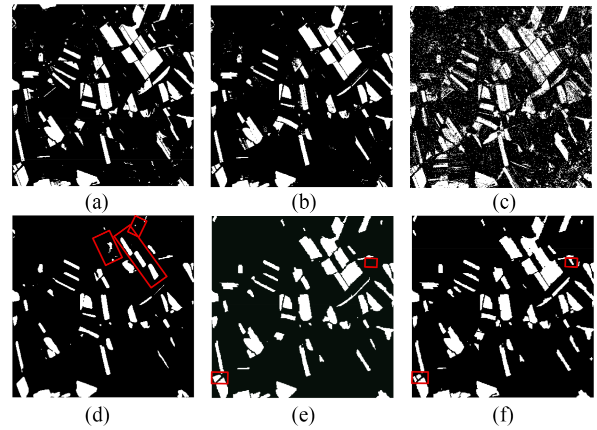

Fig. 5. CD results for dataset I. (a) CVA. (b) SFA. (c) MAD. (d) PCA-Kmeans. (e) KPVD-based. (f) MRFPCM.

TABLE I
COMPARISON BETWEEN OTHER METHODS AND THE PROPOSED MRFPCM APPROACH FOR DATASET I; THE ACCURACIES OF FA, MA, AND TE ARE PRESENTED IN PERCENTAGE (%), AND KA IS RANGED FROM 0 TO 1

Approaches	FA	MA	TE	Ka
CVA [46]	1.584	3.723	4.397	0.851
SFA [48]	0.842	6.002	5.850	0.791
MAD [47]	12.330	5.660	13.671	0.596
PCA-Kmeans [5]	0.450	11.573	10.966	0.551
KPVD-based [25]	0.767	5.078	4.951	0.826
MRFPCM	0.940	4.478	4.550	0.842

C. Experimental Results

1) Dataset I: For dataset I, the CD results are shown in Fig. 5. By comparing the visual results of the PBCD methods, the results based on CVA, SFA, and PCA-Kmeans contain less "salt-and-pepper" noise and a large amount of pretzel noise exists in the CD results based on MAD due to the low resolution of the dataset. Moreover, PCA-Kmeans performs poorly in the classification of large objects. For example, the actual change areas in the red boxes in Fig. 5(d) are larger than the detection results. The KPVD-based and MRFPCM approaches achieve an outstanding performance on removing "salt-and-pepper" noise because their basic analysis unit is a geographic object. Additionally, due to considering the uncertainty in classification, MRFPCM performs better than the KPVD-based method in small objects classification (e.g., the results in the red boxes), which also proved the feasibility of the hypothesis in Fig. 3.

Table I shows the quantitative evaluation of the results achieved based on dataset I. The results show that the MRFPCM has a performance second only to the CVA in the images with a low spatial resolution. Moreover, the OBCD approaches (KPVD-based and MRFPCM) perform better than the other PBCD approaches in general. Specifically, the MA, and TE for MRFPCM are only 0.755%, and 0.153% higher than the CVA, respectively, and are lower than the SFA (1.542% and 1.300%,

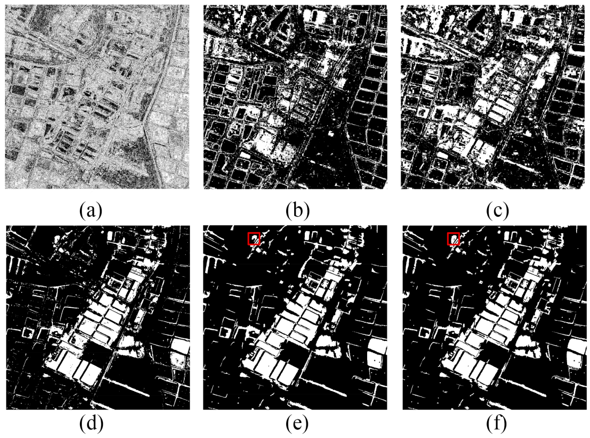

Fig. 6. CD results for dataset II. (a) CVA. (b) SFA. (c) MAD. (d) PCA-Kmeans. (e) KPVD-based. (f) MRFPCM.

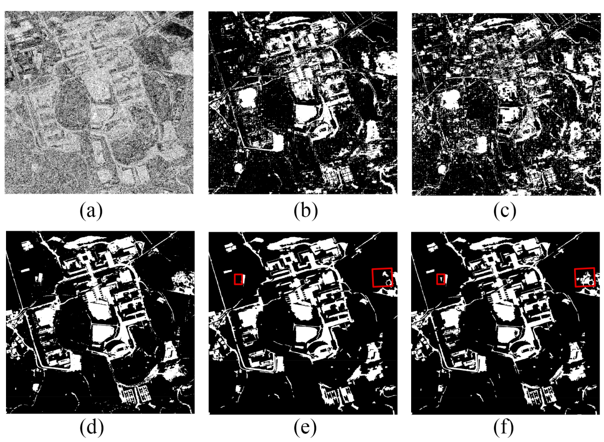

Fig. 7. CD results for dataset III. (a) CVA. (b) SFA. (c) MAD. (d) PCA-Kmeans. (e) KPVD-based. (f) MRFPCM.

respectively), MAD (1.118% and 9.121%, respectively), PCA-Kmeans (7.095% and 6.416%, respectively), and KPVD-based approaches (0.600% and 0.401%, respectively). The KA for MRFPCM are improved by 0.051, 0.246, 0.291, and 0.016 over the SFA, MAD, PCA-Kmeans, and KPVD-based methods, respectively, and is only reduced by 0.009 over the CVA. As the proposed MRFPCM approach considers contextual information and classification uncertainty, it performs better than most PBCD approaches and the other OOCD method (KPVD-based method).

2) Datasets II and III: For complex datasets II and III, the CD results are shown in Figs. 6 and 7, respectively. It can be found that CVA, SFA, and MAD perform poorly in datasets II and III due to the absence of contextual information, especially for CVA. Since PCA-Kmeans considers the pixel neighborhood relationship within the "h × h" block, and the KPVD-based and MRFPCM methods take the object as the unit of analysis, they have an excellent performance on removing "salt-and-pepper" noise. In addition, the OOCD methods (MRFPCM and KPVD-based) perform almost the same in the CD of large objects. The differences between the MRFPCM and KPVD-based approaches exist in the classification results of small objects. From the results in red boxes in Figs. 6 and 7, the MRFPCM performs better than the KPVD-based method on the classification of small objects.

TABLE II
COMPARISON BETWEEN OTHER METHODS AND THE PROPOSED MRFPCM APPROACH FOR DATASET II; THE ACCURACIES OF FA, MA, AND TE ARE PRESENTED IN PERCENTAGE (%), AND KA IS RANGED FROM 0 TO 1

Approaches	FA	MA	TE	Ka
CVA [46]	144.838	17.979	58.191	0.114
SFA [48]	24.347	14.472	28.646	0.186
MAD [47]	33.800	10.636	29.253	0.272
PCA-Kmeans [5]	8.304	7.644	12.846	0.586
KPVD-based [25]	8.385	7.038	12.339	0.606
MRFPCM	7.722	7.201	12.092	0.611

TABLE III
COMPARISON BETWEEN OTHER METHODS AND THE PROPOSED APPROACH FOR DATASET III; THE ACCURACIES OF FA, MA, AND TE ARE PRESENTED IN PERCENTAGE (%), AND KA IS RANGED FROM 0 TO 1

Approaches	FA	MA	TE	Ka
CVA [46]	103.375	16.988	48.127	0.124
SFA [48]	12.306	12.993	18.984	0.497
MAD [47]	20.793	17.050	27.186	0.308
PCA-Kmeans [5]	6.639	12.494	15.146	0.576
KPVD-based [25]	5.951	13.734	15.909	0.544
MRFPCM	5.800	13.773	15.851	0.545

To further test the feasibility of the MRFPCM, the quantitative results are presented in Tables II and III. As the complexity of the land changes increases, the performance of FA, MA, TE, and Ka decrease compared to dataset I. The results including FA, MA, TE, and Ka of CVA, SFA, and MAD are poor in datasets II and III. For dataset II, the FA, TE, and Ka based on the proposed MRFPCM method are 7.722%, 12.092%, and 0.611, respectively, which are the best accuracies compared with the other methods. For dataset III, the proposed MRFPCM performs the best with 5.800 in FA, improved by 97.575%, 6.506%, 14.933%, 0.839%, and 0.151% over CVA, SFA, MAD, PCA-Kmeans, and KPVD-based approaches. TE and Ka of the MRFPCM perform the second best with 15.851 and 0.545, which are only lower than PCA-Kmeans. Although PCA-Kmeans performs the best in MA, TE, and Ka, it shows inferior results in dataset I. It indicates that there is poor stability in the PCA-Kmeans. Compared to the KPVD-based method, the MRFPCM method can achieve better results in FA, TE, and Ka.

Based on the abovementioned experimental analysis and comparison, the MRFPCM method maintains a more stable accuracy than the PBCD methods in detecting land changes with different complexities. Meanwhile, it can extract the land changes better than the other OOCD method (KPVD-based) because the MRFPCM method takes into account the classification uncertainty.

IV. DISCUSSION

A. *Sensitivity of Different Coarsest Scales and Initial Thresholds on the Proposed MRFPCM Method*

To test the sensitivity of different parameter settings, this section explores the relationship between the coarsest scale, initial threshold, and CD accuracy (FA, MA, TE, and Ka) in

TABLE IV
PARAMETERS SETTINGS WITH THE PROPOSED MRFPCM METHOD FOR DATASET I

The coarsest scale	Initial threshold	FA	MA	TE	Ka
10	0.70	0.731	4.940	4.799	0.832
	0.75	0.730	4.848	4.716	0.835
	0.80	0.743	4.794	4.679	0.836
	0.85	0.840	4.752	4.719	0.835
	0.90	0.940	4.478	4.550	0.842
20	0.70	0.847	5.402	5.308	0.812
	0.75	0.848	5.321	5.235	0.815
	0.80	0.808	5.132	5.030	0.822
	0.85	0.786	5.216	5.091	0.821
	0.90	0.751	5.297	5.136	0.819
30	0.70	0.773	7.280	6.983	0.743
	0.75	0.684	7.282	6.914	0.745
	0.80	0.689	6.930	6.588	0.759
	0.85	0.698	6.720	6.399	0.767
	0.90	0.667	6.651	6.310	0.770
40	0.70	1.133	7.740	7.702	0.716
	0.75	1.149	7.469	7.458	0.727
	0.80	1.123	7.556	7.502	0.725
	0.85	1.001	7.650	7.517	0.722
	0.90	0.685	7.701	7.316	0.728

TABLE V
PARAMETERS SETTINGS WITH THE PROPOSED MRFPCM METHOD FOR DATASET II

The coarsest scale	Initial threshold	FA	MA	TE	Ka
30	0.70	9.055	7.299	13.031	0.587
	0.75	8.681	7.296	12.778	0.593
	0.80	8.621	7.353	12.790	0.592
	0.85	8.629	7.382	12.822	0.590
	0.90	9.243	7.293	13.151	0.584
40	0.70	8.648	7.195	12.659	0.597
	0.75	8.602	7.268	12.699	0.595
	0.80	8.463	7.399	12.726	0.592
	0.85	8.240	7.473	12.643	0.593
	0.90	7.931	7.575	12.528	0.594
50	0.70	7.722	7.201	12.038	0.611
	0.75	7.688	7.285	12.092	0.608
	0.80	7.981	7.270	12.279	0.604
	0.85	7.677	7.200	12.283	0.570
	0.90	7.541	7.534	12.222	0.602
60	0.70	8.257	6.672	12.129	0.591
	0.75	8.269	6.667	12.133	0.591
	0.80	8.210	6.673	12.098	0.592
	0.85	8.063	6.56	12.891	0.599
	0.90	6.909	7.585	11.831	0.610

TABLE VI
PARAMETERS SETTINGS WITH THE PROPOSED MRFPCM METHOD FOR DATASET III

The coarsest scale	Initial threshold	FA	MA	TE	Ka
30	0.70	5.730	13.875	15.906	0.542
	0.75	5.704	13.821	15.837	0.544
	0.80	5.512	14.083	15.972	0.538
	0.85	5.800	13.773	15.851	0.545
	0.90	5.939	13.699	15.866	0.545
40	0.70	5.522	14.027	15.923	0.539
	0.75	5.459	14.151	16.006	0.536
	0.80	5.268	14.148	15.881	0.538
	0.85	5.320	14.182	15.947	0.537
	0.90	5.373	14.206	16.004	0.535
50	0.70	5.522	14.191	16.086	0.534
	0.75	5.357	14.066	15.856	0.540
	0.80	5.464	14.981	15.841	0.542
	0.85	5.302	14.256	16.010	0.534
	0.90	5.305	14.260	16.014	0.534
60	0.70	5.768	14.471	16.521	0.521
	0.75	5.396	14.555	16.367	0.523
	0.80	5.468	14.492	16.350	0.524
	0.85	5.067	14.812	16.414	0.518
	0.90	4.972	14.749	16.290	0.521

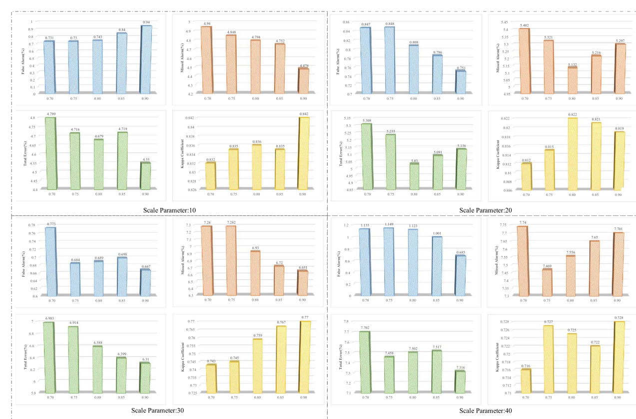

Fig. 8. Sensitivity analysis of the coarsest scale parameter and initial threshold for dataset I. The coarsest scale parameters are from 10 to 40, and the scale decay is 5. The initial thresholds are from 0.70 to 0.90, and the threshold decay is 0.50.

datasets I, II, and III. For simple and complex datasets, the coarsest segmentation scale ranges are set from 10 to 40, and 30 to 60, respectively, and the scale increases in steps of 10. Initial thresholds are set from 0.70 to 0.90, and other basic parameters are the same as described in Section III.

As shown in Tables IV, V, and VI, the setting of the coarsest scale plays an important role in the CD for datasets I, II, and III. In the test for dataset I, the lowest Ka is 0.812 when the coarsest scales are 10 and 20, while the highest Ka is 0.770 when the coarsest scales are 30 and 40. For datasets II and III, the MRFPCM method achieves the best result with the coarsest segmentation scales of 50 and 30, respectively. Therefore, it is necessary to detect a sensible coarsest segmentation before the CD based on the proposed MRFPCM is performed in the RSIs. When the selected coarsest scale is too large, a large amount of partial changed objects can be generated in the segmentation process, which will increase the uncertainties in classification and lead to a low CD. In addition, the CD results are better when the coarsest scale is small in the RSIs with a low resolution and complex land changes compared with the ones with a higher resolution and simple land changes. The best performance in the datasets I and III is achieved with the coarsest scale of 10 and 30, respectively, which are the finest scales in the tests.

To explore the effect of the initial threshold on the results, the results based on the different initial thresholds are presented in Figs. 8–10 corresponding to the datasets I, II, and III, respectively. For dataset I, at the same coarsest scale, FA, MA, and TE show a gradually decreasing trend with the increase of the initial membership threshold, while the results of Ka have an increasing trend. The reason might be that the classification for the changed and unchanged categories is stricter as the initial threshold increases, which would produce more accurate classification information at the coarsest scale. However, the performance of the MRFPC has a peak when dataset I is segmented at the coarsest scale of 20. Although more accurate classification information is produced when the initial threshold value is larger, it would lead to a decrease in the number of changed and unchanged training samples, which will make the CD accuracy decrease. There are similar situations in datasets II and III (e.g., the coarsest scales are 30 and 40 in dataset II and the coarsest scales are 40, 50, and 60).

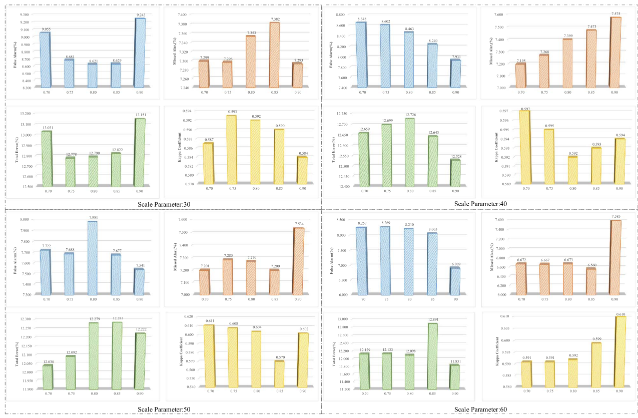

Fig. 9. Sensitivity analysis of the coarsest scale parameter and initial threshold for dataset II. The coarsest scale parameters are from 30 to 60, and the scale decay is 5. The initial thresholds are from 0.70 to 0.90, and the threshold decay is 0.50.

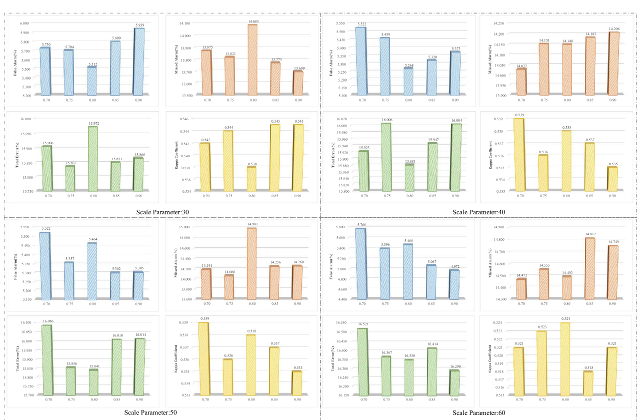

Fig. 10. Sensitivity analysis of the coarsest scale parameter and initial threshold for dataset III. The coarsest scale parameters are from 30 to 60, and the scale decay is 5. The initial thresholds are from 0.70 to 0.90, and the threshold decay is 0.50.

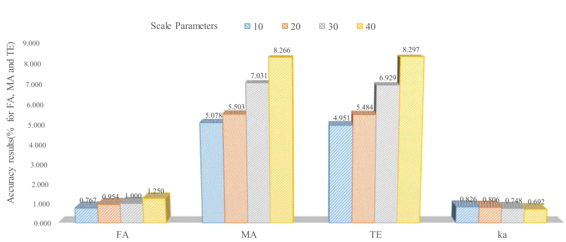

Fig. 11. Scale parameters setting with the KPVD-based approach for dataset I. Scale parameters are selected from 10 to 40 with a step size of 10.

B. Comparison of the KPVD-Based Method and Proposed MRFPCM Method With Different Parameters

The proposed MRFPCM method is improved based on the KPVD-based method by the classifier. The superiority of the two algorithms is compared in the case that the coarsest scale of the MRFPCM method was the same as that of the KPVD-based method. The results of different scale parameters with the KPVD-based method are shown in Figs. 11–13 and the results

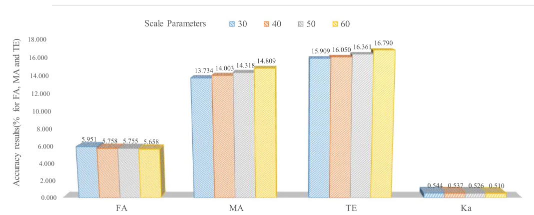

Fig. 12. Scale parameters setting with the KPVD-based approach for dataset II. Scale parameters are selected from 30 to 60 with a step size of 10.

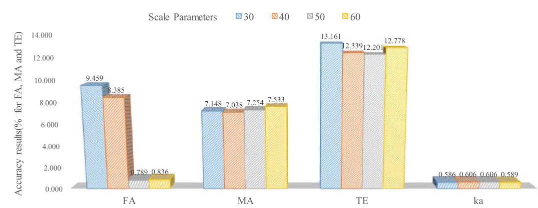

Fig. 13. Scale parameters setting with the KPVD-based approach for dataset III. Scale parameters are selected from 30 to 60 with a step size of 10.

based on the MRFPCM method are shown in Tables IV–VI, respectively.

For dataset I, the Ka of the MRFPCM approach is generally higher than the KPVD-based approach in the cases with the same coarsest scale. In addition, the FA, MA, and TE of the MRFPCM approach are mostly lower than the KPVD-based approach. The CD results in dataset I demonstrate that the proposed MRFPCM has a better performance than the KPVD-based method in the RSIs with a low resolution. For dataset II, with the coarsest scale of 40, the performance of the KPVD-based method is better than the MRFPCM method by a small margin. On other scales, the performance of the MRFPCM method is better than the KPVD-based method. For dataset III, the Ka of the MRFPCM method is higher than the KPVD-based method overall. Meanwhile, the FA, MA, and TE of the MRFPCM method also achieve better results than the KPVD-based method in the dataset. Based on the abovementioned comparison, the MRFPCM method generally performed better with the same coarsest scale.

V. Conclusion

To reduce the classification uncertainty in CD based on RSIs, this article proposed an improved RFPCM method (MRFPCM) by integrating multiresolution information. First, the multiresolution segmentation approach is employed to segment stacked images into objects from coarse to fine scales. Second, the improved RFPCM is used to classify the objects into changed, unchanged, and uncertainty categories by a shrinkable threshold T. Third, all the changed and unchanged objects at the previous scales are combined as the training sample in the proposed MRFPCM to generate new CD results at a fine scale. Finally, the RSIs are interpreted as changed and unchanged targets layer by layer until there are no uncertain objects.

Five widely used CD approaches including CVA [45], MAD [46], PCA-Kmeans [8], SFA [47], and KPVD-based [24] were compared with the MRFPCM approach in three datasets with different spatial resolution and land change complexity to verify its stability and reliability. The results show that the proposed MRFPCM can detect object changes effectively and maintain reliable accuracy in simple and complex change datasets. Meanwhile, it is found that the accuracies had a significant relationship with the coarsest scale parameters by the tests with different coarsest scale parameters and initial thresholds. If the coarsest scale is appropriately set finer, the MRFPCM can achieve a great performance in RSIs. Although a larger initial threshold can generate more accurate classification information of changed and unchanged, it brings in a decrease of training samples. Therefore, the initial threshold needs to be set in a reasonable range.

However, the performance based on the proposed method needs to be enhanced in complex land cover changes, although many algorithms are not very accurate in complex land cover changes. In future research, we will focus on the automatic coarsest scale and initial threshold selection process to improve the CD performance instead of using enumeration for selection.

References

[1] A. Singh, "Review article digital change detection techniques using remotely-sensed data," *Int. J. Remote Sens.*, vol. 10, no. 6, pp. 989–1003, 1989.

[2] A. H. Chughtai, A. H. Chughtai, and I. R. Karas, "A review on change detection method and accuracy assessment for land use land cover," *Remote Sens. Appl.: Soc. Environ.*, vol. 22, 2021, Art. no. 100482.

[3] M. A.-A. Hoque, S. Phinn, C. Roelfsema, and I. Childs, "Tropical cyclone disaster management using remote sensing and spatial analysis: A review," *Int. J. Disaster Risk Reduction*, vol. 22, pp. 345–354, Jun. 2017.

[4] X.-L. Chen, H.-M. Zhao, P.-X. Li, and Z.-Y. Yin, "Remote sensing image-based analysis of the relationship between urban heat island and land use/cover changes," *Remote Sens. Environ.*, vol. 104, no. 2, pp. 133–146, Sep. 2006.

[5] J. C. White, N. C. Coops, M. A. Wulder, M. Vastaranta, T. Hilker, and P. Tompalski, "Remote sensing technologies for enhancing forest inventories: A review," *Can. J. Remote Sens.*, vol. 42, no. 5, pp. 619–641, Sep. 2016.

[6] L. Bruzzone and D. Prieto, "Automatic analysis of the difference image for unsupervised change detection," *IEEE Trans. Geosci. Remote Sens.*, vol. 38, no. 3, pp. 1171–1182, May 2000.

[7] D. Lu, P. Mausel, E. Brondizio, and E. Moran, "Change detection techniques," *Int. J. Remote Sens.*, vol. 25, no. 12, pp. 2365–2401, 2003.

[8] T. Celik, "Unsupervised change detection in satellite images using principal component analysis and k-means clustering," *IEEE Geosci. Remote Sens. Lett.*, vol. 6, no. 4, pp. 772–776, Oct. 2009.

[9] W. Shi, M. Zhang, R. Zhang, S. Chen, and Z. Zhan, "Change detection based on artificial intelligence: State-of-the-art and challenges," *Remote Sens.*, vol. 12, no. 10, May 2020, Art. no. 1688.

[10] L. ZhiYong et al., "Diagnostic analysis on change vector analysis methods for LCCD using remote sensing images," *IEEE J. Sel. Topics Appl. Earth Observ. Remote Sens.*, vol. 14, pp. 10199–10212, Sep. 2021.

[11] Z. Lv et al., "Land cover change detection with heterogeneous remote sensing images: Review, progress, and perspective," *Proc. IEEE*, pp. 1–16, Nov. 2022, doi: 10.1109/JPROC.2022.3219376.

[12] W. Shi and P. Zhang, "Stateoftheart remotely sensed images-based change detection methods," *Geomatics Inf. Sci. Wuhan Univ.*, vol. 13, no. 25, pp. 8461–8481, 2018.

[13] Z. Lv, G. Li, Z. Jin, J. A. Benediktsson, and G. M. Foody, "Iterative training sample expansion to increase and balance the accuracy of land classification from VHR imagery," *IEEE Trans. Geosci. Remote Sens.*, vol. 59, no. 1, pp. 139–150, Jan. 2021.

[14] J. Zhang, Q. Yu, and J. Hou, "Object-oriented classification and information extraction based on high spatial resolution remote sensing image," *Remote Sens. Technol. Appl.*, vol. 25, no. 1, pp. 112–117, 2010.

[15] Z. Lv, F. Wang, G. Cui, J. A. Benediktsson, T. Lei, and W. Sun, "Spatial attention network guided with change magnitude image for land cover change detection using remote sensing images," *IEEE Trans. Geosci. Remote Sens.*, vol. 60, pp. 1–12, Aug. 2022.

[16] J. Im and J. R. Jensen, "A change detection model based on neighborhood correlation image analysis and decision tree classification," *Remote Sens. Environ.*, vol. 99, no. 3, pp. 326–340, 2005.

[17] P. Xiao, M. Yuan, X. Zhang, X. Feng, and Y. Guo, "Cosegmentation for object-based building change detection from high-resolution remotely sensed images," *IEEE Trans. Geosci. Remote Sens.*, vol. 55, no. 3, pp. 1587–1603, Mar. 2017.

[18] G. Hazel, "Object-level change detection in spectral imagery," *IEEE Trans. Geosci. Remote Sens.*, vol. 39, no. 3, pp. 553–561, Mar. 2001.

[19] M. Zhang and W. Shi, "A feature difference convolutional neural network-based change detection method," *IEEE Trans. Geosci. Remote Sens.*, vol. 58, no. 10, pp. 7232–7246, Oct. 2020.

[20] K. Chen, C. Huo, J. Cheng, Z. Zhou, and H. Lu, "Change detection based on adaptive Markov random fields," in *Proc. 19th Int. Conf. Pattern Recognit.*, 2008, pp. 1–4.

[21] D. Feng, X. Shen, Y. Xie, Y. Liu, and J. Wang, "Efficient occluded road extraction from high-resolution remote sensing imagery," *Remote Sens.*, vol. 13, no. 24, 2021, Art. no. 4974.

[22] M. Gong, Y. Yang, T. Zhan, X. Niu, and S. Li, "A generative discriminatory classified network for change detection in multispectral imagery," *IEEE J. Sel. Topics Appl. Earth Observ. Remote Sens.*, vol. 12, no. 1, pp. 321–333, Jan. 2019.

[23] W. Gu, Z. Lv, and M. Hao, "Change detection method for remote sensing images based on an improved Markov random field," *Multimedia Tools Appl.*, vol. 76, no. 17, pp. 17719–17734, Sep. 2017.

[24] Z. Lv, T. Liu, and J. A. Benediktsson, "Object-oriented key point vector distance for binary land cover change detection using VHR remote sensing images," *IEEE Trans. Geosci. Remote Sens.*, vol. 58, no. 9, pp. 6524–6533, Sep. 2020.

[25] P. Lv, Y. Zhong, J. Zhao, and L. Zhang, "Unsupervised change detection based on hybrid conditional random field model for high spatial resolution remote sensing imagery," *IEEE Trans. Geosci. Remote Sens.*, vol. 56, no. 7, pp. 4002–4015, Jul. 2018.

[26] Y. Cheng, "Mean shift, mode seeking, and clustering," *IEEE Trans. Pattern Anal. Mach. Intell.*, vol. 17, no. 8, pp. 790–799, Aug. 1995.

[27] S. Ryherd and C. Woodcock, "Combining spectral and texture data in the segmentation of remotely sensed images," *Photogrammetric Eng. Remote Sens.*, vol. 62, no. 2, pp. 181–194, 1996.

[28] U. C. Benz, P. Hofmann, G. Willhauck, I. Lingenfelder, and M. Heynen, "Multi-resolution, object-oriented fuzzy analysis of remote sensing data for GIS-ready information," *ISPRS J. Photogrammetry Remote Sens.*, vol. 58, no. 3, pp. 239–258, Jan. 2004. .

[29] L. Drăguţ, D. Tiede, and S. R. Levick, "ESP: A tool to estimate scale parameter for multiresolution image segmentation of remotely sensed data," *Int. J. Geographical Inf. Sci.*, vol. 24, no. 6, pp. 859–871, Apr. 2010.

[30] L. Drăguţ, O. Csillik, C. Eisank, and D. Tiede, "Automated parameterisation for multi-scale image segmentation on multiple layers," *ISPRS J. Photogrammetry Remote Sens.*, vol. 88, pp. 119–127, Feb. 2014.

[31] V. A. Ayma Quirita et al., "Metaheuristics for supervised parameter tuning of multiresolution segmentation," *IEEE Geosci. Remote Sens. Lett.*, vol. 13, no. 9, pp. 1364–1368, Sep. 2016.

[32] Y. Chen, M. Dongping, L. Xu, and L. Zhao, "An overview of quantitative experimental methods for segmentation evaluation of high spatial remote sensing images," *J. Geo-Inf. Sci.*, vol. 19, no. 6, pp. 818–830, 2017.

[33] M. Hao, W. Shi, K. Deng, H. Zhang, and P. He, "An object-based change detection approach using uncertainty analysis for VHR images," *J. Sensors*, vol. 2016, pp. 1–17, 2016.

[34] Y. Zhang, D. Peng, and X. Huang, "Object-based change detection for VHR images based on multiscale uncertainty analysis," *IEEE Geosci. Remote Sens. Lett.*, vol. 15, no. 1, pp. 13–17, Jan. 2018.

[35] J. Kapur, P. Sahoo, and A. Wong, "A new method for gray-level picture thresholding using the entropy of the histogram," *Comput. Vis., Graph., Image Process.*, vol. 29, no. 3, pp. 273–285, 1985.

[36] L.-K. Huang and M.-J. J. Wang, "Image thresholding by minimizing the measures of fuzziness," *Pattern Recognit.*, vol. 28, no. 1, pp. 41–51, 1995.

[37] N. Otsu, "A threshold selection method from gray-level histograms," *IEEE Trans. Syst., Man Cybern.*, vol. SMC-9, no. 1, pp. 62–66, Jan. 1979.

[38] L. Huang, Y. Fang, X. Zuo, and X. Yu, "Automatic change detection method of multitemporal remote sensing images based on 2D-Otsu algorithm improved by firefly algorithm," *J. Sensors*, vol. 2015, no. 3, pp. 1–8, 2015.

[39] Z. Lv, T. Liu, J. Atli Benediktsson, T. Lei, and Y. Wan, "Multi-scale object histogram distance for LCCD using bi-temporal very-high-resolution remote sensing images," *Remote Sens.*, vol. 10, no. 11, Nov. 2018, Art. no. 1809.

[40] K. Wagstaff, C. Cardie, S. Rogers, and S. Schrödl, "Constrained k-means clustering with background knowledge," in *Proc. 18th Int. Conf. Mach. Learn.*, 2001, pp. 577–584.

[41] J. Warner, "Scikit-fuzzy," 2019. [Online]. Available: https://github.com/JDWarner/scikit-fuzzy

[42] C. E. Rasmussen, "The infinite Gaussian mixture model," in *Proc. Adv. Neural Inf. Process. Syst.*, vol. 12, no. 4, pp. 554–560, 2000.

[43] U. H. Atasever, M. A. Gunen, and E. Besdok, "A new unsupervised change detection approach based on PCA based blocking and GMM clustering for detecting flood damage," *Fresenius Environ. Bull.*, vol. 27, no. 3, pp. 1688–1694, 2018.

[44] D. Miao, Z. Wei, R. Wang, C. Zhao, Y. Chen, and X. Zhang, *Uncertainty Analysis in Granular Computing*. Beijing, China: Science Press, 2019.

[45] F. Bovolo and L. Bruzzone, "A theoretical framework for unsupervised change detection based on change vector analysis in the polar domain," *IEEE Trans. Geosci. Remote Sens.*, vol. 45, no. 1, pp. 218–236, Jan. 2007.

[46] A. A. Nielsen, K. Conradsen, and J. J. Simpson, "Multivariate alteration detection (MAD) and maf postprocessing in multispectral, bitemporal image data: New approaches to change detection studies," *Remote Sens. Environ.*, vol. 64, no. 1, pp. 1–19, Apr. 1998.

[47] C. Wu, B. Du, and L. Zhang, "Slow feature analysis for change detection in multispectral imagery," *IEEE Trans. Geosci. Remote Sens.*, vol. 52, no. 5, pp. 2858–2874, May 2014.

[48] C. Munyati, "Optimising multiresolution segmentation: Delineating savannah vegetation boundaries in the Kruger National Park, South Africa, using sentinel 2 MSI imagery," *Int. J. Remote Sens.*, vol. 39, no. 18, pp. 5997–6019, Sep. 2018.

[49] L. spatial discover, "Multi-resolution segmentation," 2022. [Online]. Available: http://learningzone.rspsoc.org.uk/index.php/Learning-Materials/Object-oriented-Classification/2.5.-Multi-Resolution-Segmentation

[50] W. Ma, L. Jiao, M. Gong, and C. Li, "Image change detection based on an improved rough fuzzy c-means clustering algorithm," *Int. J. Mach. Learn. Cybern.*, vol. 5, no. 3, pp. 369–377, Jun. 2014.

[51] Z. Pawlak, "Rough sets," *Int. J. Comput. Inf. Sci.*, vol. 11, pp. 341–356, 1982.

[52] A. A. Nielsen, "Multi-channel remote sensing data and orthogonal transformations for change detection," in *Machine Vision and Advanced Image Processing in Remote Sensing*, I. Kanellopoulos, G. G. Wilkinson, and T. Moons, Eds. Berlin, Germany: Springer, 1999, pp. 37–48.

Tong Xiao received the B.S. degree in geographic information science (GIS) in 2019 from the School of Geographical Sciences, Hunan Normal University, Changsha, China, where he is currently working toward the M.Sc. degree in GIS.

His research interests include the uncertainty of crowdsourced data using granular computing and machine learning methods.

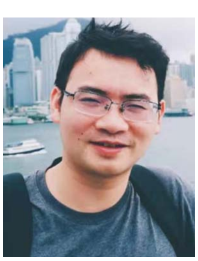

Yiliang Wan received the B.S. degree in remote sensing science and technology and the Ph.D. degree in photogrammetry and remote sensing from Wuhan University, Wuhan, China, in 2009 and 2015, respectively.

He is currently an Associate Professor with the School of Geographical Sciences, Hunan Normal University, Changsha, China. His research interests include land use processing and applications, and spatial uncertainty modeling.

Jianjun Chen received the Ph.D. degree in environmental science from the Graduate School of Chinese Academy of Sciences, Beijing, China, in 2005.

He is currently a Professor with the Hunan Vocational College of Engineering, Changsha, China. His research interests include application of remote sensing technology, thematic map design, land-cover and land-use change, and urban landscape ecology.

Wenzhong Shi received the Doctoral degree in surveying and mapping from the University of Osnabruck, Vechta, Germany, in 1994.

He is currently the Director of Otto Poon Charitable Foundation Smart Cities Research Institute, PolyU, Hong Kong, Director of PolyU-Shenzhen Technology and Innovation Research Institute (Futian), Chair Professor in Geographic Science and Remote Sensing, and Director of Joint Research Laboratory on Spatial Information, PolyU and Wuhan University, Wuhan, China. He is an Academician of International Eurasian Academy of Sciences and a Fellow of Academy of Social Sciences (U.K.). His research interests include GISci, remote sensing and urban informatics, with focusing on analytics and quality control for spatial Big Data, object extraction and change detection from satellite images and LiDAR data, integrated indoor mapping technology, 3-D and dynamic GISci modeling, and smart city applications.

Prof. Shi is currently a Fellow of Royal Institution of Chartered Surveyors and Hong Kong Institute of Surveyors. He is also a President of International Society for Urban Informatics and Editor-in-Chief of *International Journal Urban Informatics*.

Jianxin Qin received the B.S. degree in geography education from Hunan Normal University, Changsha, China, in 1992, and the M.S. degree in physical geography from Peking University, Beijing, China, in 1997, and the Ph.D. degree in cartography and geography information system from the Chinese Academy of Science, Beijing, China, in 2000.

He is currently a Professor of Cartography and Geography Information System, Hunan Normal University, Changsha, China. His research is focused on visualization of spatial information, spatial information system, and spatial data mining.

Deping Li received the B.S. degree in geology from the Department of Geology, Nanjing University, Nanjing, China, in 1986, and the Ph.D. degree in geoscience from the Department of Earth Sciences, Nanjing University, in 2003.

He is currently a Professor with the School of Geographical Sciences, Hunan Normal University, Changsha, China. His research interests include spatial decision support technology, mineral resource prediction and evaluation, GIS application software development, deep-sea informatics, and other computer technology applications in geology.